Numerical Simulation of Arc and Metal Transfer in Arc Welding Based Additive Manufacturing Assisted by External Longitudinal Static Magnetic Field

Xiangman Zhou (zhouxman@ctgu.edu.cn)
College of Mechanical and Power Engineering, China Three Gorges University, Yichang 443002, China
https://orcid.org/0000-0003-2260-8722

Lian Liu
China Three Gorges University

Boyun Wang
China Three Gorges University

Xingwang Bai
University of South China

Haiou Zhang
Huazhong University of Science and Technology

Qihua Tian
China Three Gorges University

Yixian Du
China Three Gorges University

Original Article

Keywords: arc welding based additive manufacturing, external longitudinal static magnetic field, numerical simulation, surface quality

Posted Date: July 30th, 2020

DOI: https://doi.org/10.21203/rs.3.rs-50252/v1

Abstract

The surface quality is one of important quality factors for arc welding based additive manufacturing (AWAM) parts. In this study, AWAM process assisted by an external longitudinal static magnetic field (ELSMF) is applied to improve surface quality of AWAM parts. In order to study the internal mechanism of AWAM process assisted by an external longitudinal magnetic field, a three-dimensional weak coupling model of the arc and metal transport is developed to simulate the arc, molten pool dynamic in AWAM assisted by ELSMF. The simulated results of single-bead deposition show that the ELSMF induces the asymmetrical tangential electromagnetic stirring in arc and molten pool, which can increase molten pool dynamics, drive the molten metal moving to the edge of the molten pool and reduce the temperature gradient. The simulated results of overlapping deposition show that the asymmetrical tangential electromagnetic stirring force can drive the molten metal moving to valley area between overlapping beads, which is beneficial to filling the valley area and improving the surface quality of the AWAM parts. The single-bead deposition experiment shows that the applying of ELSMF can reduce the height as well as increase the width of single weld bead. The multi-bead overlapping and the multi-layer multi-pass deposition experiments demonstrate that the external magnetic field can improve the surface quality of multi-layer part. The conclusions of the above study can provide the reference for AWAM process assisted by magnetic field.

1. Introduction

Arc welding based additive manufacturing (AWAM) is an innovative metallic additive manufacturing (AM) technology using arc welding as heat source and wire as consumable materials. Compared with laser or electron beam based AM technology, the AWAM technology has the advantage of lower cost, higher energy efficiency and deposition rate[1]. The AWAM technology has been demonstrated to be a popular technique for fabricating large and complex components in aerospace and warships field in the future [2].

As a result of the lower resolution of arc welding bead, the AWAM parts have the inferior surface quality, which has critical effects on the deposition defects, geometric error, and dimensional accuracy of metallic parts in layered deposition process. To address this problem, many scholars have come up with some ways to improve the surface quality for AWAM parts. Fu, et al[3], established a multi-objective optimization process by using the Box-Behnken design of response surface methodology for Bainite steel additive manufacturing. The optimization process enables the capacity of fabricating metal parts with high accuracy and lays a good foundation for Bainite steel additive manufacturing. Xiong and Zhang[4], also developed a passive vision sensor and adaptive control system to monitor the nozzle to the top surface distance(NTSD) in AWAM process. This system can keep the constant NTSD by moving the working flat and adjusting the deposition rate on next deposition layer, which can improve process stability and obtain smooth thin-walled parts. Recently, Li, et al[5], proposed a new layers-overlapping strategy which considered the geometric area of adjacent beads and the spreading of the melted weld

beads. The confirmatory experiments demonstrated that the proposed strategy could improve the surface flatness of layers of multi-layer and multi-bead parts produced by AWAM as well as prevent formation of defects inside the parts. The above works improve the surface quality of AWAM parts by means of bead modeling and process parameter optimization. But these strategies are all belonging to a passive strategy. Other researchers combined the in-situ milling[6] or in-situ rolling[7] into the AWAM process to directly improve the surface quality of AWAM parts. But, these hybrid methods require CNC machine support which will greatly increase the equipment cost and control difficulty.

The external electromagnetic field has been widely employed in AWAM or arc welding. To combat residual stress, deformation, crack, and flow-down or collapse of liquid metal of overhanging structure and tilting structure, induction heating and electromagnetic force of high-frequency magnetic field was introduced into AWAM process as a controlled thermal intervention or an electromagnetic support[8]. The longitudinal alternating or static magnetic field was introduced into gas metal arc welding (GMAW) process to analyze the stress and motion state of droplet in MIG welding[9, 23]. The transverse static magnetic field was also used to suppress the hump in the high speed welding process[10]. In these electromagnetic-assisted AWAM process, the electromagnetic stirring (EMS) is regarded as one of the main influencing factors in the deposition process. The EMS can affect the heat transfer and flow of the molten pool, thus changing the weld bead morphology and solidification crystallization. Especially, the external longitudinal static magnetic field (ELSMF) can induce EMS in arc welding deposition, which can reduce the height of weld bead as well as increase the width of weld bead, namely the increase of the aspect ratio (width-height ratio) of single weld bead. In the AWAM process, it has been demonstrated that parameter control is difficult to achieve the ideally flat surface in overlapping deposition process, and the large aspect ratio is beneficial to improve the overlapping accuracy[11]. Furthermore, the transverse cross-section of weld bead assisted by longitudinal static magnetic field is not symmetrical and tilt to one side due to the tangential-EMS and asymmetrical molten pool[12]. Figure 1 shows the schematic representation of molten pool and weld bead in arc welding deposition assisted by the external longitudinal static magnetic field. Apparently, the changes of weld bead morphology in above presentation are beneficial to improve the overlapping accuracy as well as the surface quality for multi-beads deposition in AWAM. Consequently, AWAM process assisted by an external longitudinal static magnetic field (ELSMF) is employed to improve surface quality of AWAM parts in this study.

Some scholars have been devoted to researching the arc welding or AWAM process by experiments or simulations. For instance, Chang, et al[13], introduced different kinds of external electro-magnetic fields to gas metal arc welding(GMAW) to confirm that the metal transfer frequency was improved, and spatter generation rate was diminished under controls of external electromagnetic fields by experiment. Yin, et al[14], established a 3D numerical model containing the welding arc and the weld pool for gas tungsten arc welding (GTAW) with applied axial magnetic fields to clarify the mechanism of how the applied axial magnetic field controls the GTAW process by simulation. Although experimental observations can provide some invaluable information, it is difficult to reveal the underlying mechanisms during the arc welding process due to the extremely high temperature and high velocity[15]. Numerical simulation provides a

feasible method to obtain insightful information. There are three main types of mathematical model on heat and mass transfer in arc welding or AWAM process: unified model, separated model and weak coupling mode. The unified model takes the arc, molten pool in a unified solution domain and establish a unified mathematical model, thus the interaction between the arc and molten pool can be simulated. However, the modeling and calculation processes are complex and time-consuming, and physical mechanism of the sheath area are not completely understood. Therefore, a lot of simplifications are usually introduced in unified model[16]. For instance, Xu, et al[17], developed an integrated comprehensive 3D model to study the transport phenomena in gas metal arc welding (GMAW). The separated model also has been extensively used in AWAM simulation process. As a result of the model of arc and metal transport are not simulated concurrently, the complex energy and momentum boundary conditions between the arc and the metal do not need to calculate directly. For instance, Bai, et al[18], established a separated model for AWAM process assisted by high-frequency magnetic field and the effect of mechanism of high-frequency magnetic field on heat transfer, convection and weld pool shape were analyzed. In Bai's model, the arc was supposed to be solid and the electromagnetic force was calculated by the finite element method. In our previous studies, Zhou, et al[19], developed a three-dimensional weak coupling modeling method of the arc and metal transport to simulate the arc, molten pool dynamic and droplet impingement in arc welding based additive manufacturing, and verified the stability of this weak coupling modeling method to simulating the complex heat and mass transfer phenomena in arc welding based additive manufacturing. Compared with the unified model and separated model, a three-dimensional weak coupling model has superior accuracy and lower computational consumption.

In this study, a three-dimensional weak coupling model of the arc and metal transport is developed to simulate the arc, molten pool dynamic in GMAW based additive manufacturing assisted by ELSMF. Both the single-bead deposition and overlapping deposition in the presence of ELSMF are simulated to study the effect of ELSMF on weld bead topography and overlapping accuracy.

2. Numerical Models

A weak coupling model has been developed and verified in the author's previous research[19, 22], so it will not be described in detail in this article. In this study, the weak coupling model is applied to simulate the arc and metal transport in AWAM process assisted by ELSMF.

2.1 Arc models

As shown in Fig. 2, arc model and the molten pool are simplified to be solid state. The distance between wire tip and substrate is 5 mm, the bead width is 10 mm and the bead height is 3 mm under the used process parameters (as shown in Table 1). The deposition direction is the positive direction of the x-axis. In the Fig. 2, J represents current density, **Bz**- represents the magnetic flux density of ELSMF, and **Fm** represents electromagnetic force induced by ELSMF. It can be seen that the electromagnetic force presents a tangential distribution at every point in the arc. The distribution of inducing electromagnetic force in the molten pool is similar to the arc.

The deposition process is shown in Table 1. The shielding gas is argon, and the material of the substrate and the wire is mild steel. Zhou, et al[20], shows the physical properties of argon and mild steel.

Table 1
Deposition process parameters

Parameters	Value(unit)
Deposition current	200 A
Deposition voltage	23 V
Deposition speed	530 mm/min
Wire feeding rate	6 m/min
Shielding gas flow rate	15 L/min
Ambient temperature	300 K
Wire diameter	1.6 mm
External magnetic field	0.014 T

2.2 Metal transport models

The diagrammatic sketch of metal transport models are showed in Fig. 3. The surface IJLK is the free surface of molten pool. The electromagnetic force, arc pressure, plasma shear stress and heat flux are extracted from the arc simulation and transmitted to the metal transport model.

3. Simulated Results And Discussions

3. Simulated results and discussions

3.1 Single-bead deposition

Fig. 4 reveals the simulated results of arc temperature (at plane of X=0) and molten pool electromagnetic force(at Z=0 plane) of single-bead deposition. It can be seen from Fig. 4(a) that the temperature field and electromagnetic force of molten pool are symmetric distribution in normal single-bead deposition. It can also be seen from Fig. 4(b) that in the presence of ELSMF, the arc temperature field is no longer symmetrical distribution and significantlyexpanded near the substrate, the high temperature region of arc center is enlarged, and the contact area between the arc and the metalis also increased, so that the heat transfer is more uniform. And, the electromagnetic force vector distribution of the Z=0 plane in the molten pool becomes a vortex-like aggregation with a tangential component(as shown in Fig. 4(b)) from the edge of the molten pool to the center(as shown in Fig. 4(a)), which is known as EMS in the presence of ELSMF.

Fig. 5 shows the simulated results of arc pressure (at plane of X=0). It can be seen that in the presence of ELSMF, the peak pressure of the arc is significantly reduced, and the negative pressure region appears in the center of the arc, especially the arc pressure on the surface of the molten pool is reduced and is no longer symmetrical.

Fig. 6 displays the temperature and velocity vector distribution (at plane of Y=0 mm and Z=-1 mm) of single-bead molten pool at different instants. Fig. 6(a~f) display the normal single-bead deposition results, and Fig. 6(g~l) display the single-bead deposition results in the presence of ELSMF. From the temperature field distribution of the Z=-1mm plane, it can be seen that the temperature distribution of the molten pool is no longer symmetrical when the ELSMF is applied. The velocity vector distribution indicates that the molten pool is driven by the tangential electromagnetic force which make the molten metal asymmetrically rotational in the molten pool, and increase the width (diameter in the y-axis) of the weld pool.To sum up, the tangential-EMS in the molten pool weakens the metal transport to rear of the molten pool, and enhances the metal transport to both sides (direction of the y-axis) of the molten pool, which will reduce the height as well as increase the width of single weld bead.

Fig. 7 illustrates the diagrammatic sketch of Path 1 on the Z=-1 mm plane. Fig. 8 shows the distributions of temperature and velocity on path 1 at different instants. Fig. 8(a~c) show the normal single-bead deposition results, and Fig. 8(d~f) show the single-bead deposition results in the presence of ELSMF. From the Fig.8(a) and Fig. 8(d), it can be seen that the temperature on the Path 1 is no longer symmetrically distributed in the presence of ELSMF, and the width of the molten pool on the Path 1 (the distance between the liquidus temperatures) is significantly larger than he normal single-bead deposition (as shown in Fig. 8(a)). After the comparison of Fig. 8(b) and Fig. 8(e), it can be seen that molten pool dynamics significantly increase, and the velocity magnitude no longer completely symmetrically distributed on the Path 1 in the presence of ELSMF. The tangential-velocity comparison on Path 1 shows that the molten pool has no obvious tangential motion (as shown in Fig. 8(c)), but the molten pool has significant tangential motion when applying the ELSMF (as shown in Fig.8(f)). Meanwhile, it can be seen from Fig. 8(f) that the tangential motion of the molten pool is asymmetrical, which is consistent with Fig. 6 (g~l).

3.2 Overlapping deposition

Fig. 9 illustrates the simulated results of arc temperature (at plane of X=0) and molten pool electromagnetic force (at Z=0 plane) of overlapping deposition. After the comparison of Fig. 9(a) and Fig. 9(b), it can be seen that the arc is compressed near the substrate and deposition bead in the presence of ELSMF, and the electromagnetic force vector distribution of the Z=0 plane in the molten pool also becomes a vortex-like aggregation with a tangential component(as shown in Fig. 9(b)) from the edge of the molten pool to the center(as shown in Fig. 9(a)).

Fig. 10 illustrates the temperature and velocity vector distribution (at plane of Y=0 mm, Z=-1 mm and X=0 mm) of overlapping molten pool at different instants. Fig. 10(a~f) display the normal overlapping deposition results, and Fig. 10(g~l) display the overlapping deposition results in the presence of ELSMF.

Comparing with the normal overlapping deposition, the molten pool movement is more intense and the tangential-EMS makes the weld pool temperature field distribution more uniform when applying the ELSMF. It can be seen from the Z=-1 mm and X=0 plane that the applied longitudinal static magnetic field makes the tendency of moving to the right side of the formed bead for the molten metal more obvious, which is beneficial to filling the valley area between the two overlapping welds, improving the overlapping precision and the surface quality of deposition layers.

Fig. 11 shows the distributions of temperature and velocity on Path 1 at different instants. Fig. 11(a~d) show the normaloverlapping deposition results, and Fig. 11(e~h) show the overlapping deposition results in the presence of ELSMF. From the Fig. 11(a) and Fig. 11(e), it can be indicated that the temperature at the center of molten pool is not always rising from 0.02s to 0.04s in the presence of ELSMF, the peak temperature on the Path 1 of 0.04s is lower than 0.032s~0.036s, which is result from EMS induced by the external magnetic field. So, the heat which is transferred to the molten pool would become quicker.As presented in Fig. 11(b) and Fig. 11(f), the velocity magnitude distribution on Path 1 is significantly increased when applying the ELSMF. From Fig. 11(c) and Fig. 11(g), the comparison of tangential - velocity shows that the molten pool exhibits significant tangential motion in the presence of ELSMF. After the comparison of Fig. 11(d) and Fig. 11(h), it reveals that the molten metal in molten poolmainly flows to the side without the weld bead in normal overlapping deposition, but the molten metal mainly flows to the side of the weld bead in the presence of ELSMF.

From the analysis conclusions of Fig. (6), Fig. (8), Fig. (10) and Fig. (11), it can be known that the effect of EMS induced by longitudinal magnetic field is beneficial to expanding the molten pool and reducing the temperature gradient of the molten pool. Then, the stirring effect can increase the aspect ratio(width-height ratio) of single weld bead. In the overlapping deposition, it is capable of making the molten metal flowing to the side of the weld bead and filling the valley area between the two overlapping welds. It has been demonstrated in the AWAM process that parameter control is difficult to obtain the ideally flat surface by overlapping deposition, and the large aspect ratio is beneficial to improve the overlapping precision. Therefore, the changes of molten pool flow and weld bead morphology in above presentation are beneficial to improving the overlapping accuracy as well as the surface quality for multi-beads deposition in AWAM process. The schematic diagram of cross-section profile of weld bead changes inoverlapping deposition assisted by longitudinal magnetic field are illustrated in Fig.12. In the Fig.(12), d represents center distance of two overlapping beads, h represents bead height and w represents bead width. Fig.12 (a) shows the ideal cross-section profile of overlapping weld bead under the optimized center distance, which has the symmetrical topography. But the actual cross-section profile of overlapping weld bead is shown in Fig. 12(b), which is because even under the optimized center distance, it is impossible to obtain a completely flat, symmetrical topography due to the rapid cooling and the high viscosity of the liquid metal. Especially, the weld bead has the relatively small aspect ratio in normal overlapping deposition, and the liquid metal is difficult to filling the valley area during the deposition process. The aspect ratio of weld bead becomes larger and the valley area becomes more gradual when the ELSMF is applied (as shown in Fig. 12(c)). Additionally, the EMS is beneficial to filling the valley area,

thus it is capable of improving the overlapping accuracy as well as the surface quality of multi-beads deposition.

4. Experiments

As showed in Fig. 13, an AWAM experimental setup assisted by ELSMF is put up to carry out the experiment in this study. A Motoman robot is used to execute deposition trajectory and a SAF GMAW welder is used as heat source. A coaxial excitation coil with the torch is used for applying a longitudinal magnetic field and a DC (direct current) power supply is used as excitation power supply. The deposition process parameters are the same as numerical simulations(as listed in Table 1).

According to Xiong, et al[21], as the ratio of the wire feed rate to the welding speed (RWFRTWS) is less than 12.5, the cross-section profile of weld bead should be fitted with a parabola curve, and the optimal center distance d of overlapping beads is equal to $2w/3$. In this study, RWFRTWS is equal to 11.32, thus a parabolic model is used to fit the cross-section profile of the single weld bead. When the longitudinal static magnetic field is applied, the topography, height and width of the weld bead are changed. However, the parabolic model is still the fittest model for the cross-section profile of weld bead in this study. So,allthe optimal center distance d of overlapping beads in this study is equal to $2w/3$.

Fig. 14 shows the cross-section of single-pass and multi-pass deposition. The weld bead at left side and right side in Fig.14 (a) are the cross-section of the normal single-bead deposition and single-bead deposition assisted by a longitudinal static magnetic field respectively. Fig.14 (b) and Fig.14 (c) are the four pass overlapping beads of normal deposition andfour pass overlapping beads deposition assisted by longitudinal static magnetic field respectively. The cross-section profile dimensions of weld beads and the aspect ratio of single weld bead are listed in Table 2. As can be seen from Fig. 14 and Table 2, deposition assistedbythe longitudinal static magnetic field can reduce the height and increase the width of single bead, thus significantly increase the aspect ratio of single weld bead, which result fromEMS induced by longitudinal magnetic field. After the comparison of Fig. 14(b) and Fig. 14(c), it can be seen that with the increasing of overlapping pass(from the left to the right), the topography of the overlapping beads of normal deposition changes greatly, but entire overlapping beads deposition assisted by thelongitudinal static magnetic field is flatter, which is due to process characteristic limitation of AWAM. It is difficult to obtain an ideally, completely flat overlapping beads by adjusting the process parameters, and the large aspect ratio of weld bead is beneficial to improving the overlapping precision.

Table 2 the cross-section profile dimensions of weld beads

Items	Single weld bead		The width of four pass overlapping deposition(mm)	The aspect ratioof single weld bead
	Height(mm)	Width(mm)		
Normal deposition	2.5	8	22	3.2
Depositionassisted by the longitudinal static magnetic field	2	10	27	5

Fig. 15 shows comparsion of surface topography of multi-layer multi-pass specimens(3 layers 13 passess) fabricated by normal deposition and deposition assisted by the longitudinal static magnetic field. It can be seen from Fig. 15 that the surface of the top layer of deposition assisted by the longitudinal static magnetic field is flatter, and the surface quality is improved. The frist reason is the above-described large aspect ratio of weld bead deposition assisted by the longitudinal static magnetic field and filling effect of valley area caused by EMS, and the second reason is that the improvement of the surface quality of each layer during the multi-layer deposition,which is beneficial to reducing theaccumulated errors between the layers and enables subsequent layers to continue to achieve high surface quality.

5. Conclusions

(1) The asymmetrical tangential electromagnetic stirring force induced by ELSMF in molten pool which can increase molten pool dynamics, drive the molten metal moving to the edge of the molten pool, and reduce the temperature gradient.

(2) The simulated results of overlapping deposition show that the asymmetrical tangential electromagnetic stirring force can drive the molten metal moving to valley area between the overlapping beads, which is beneficial to filling the valley area and improving the surface quality of the AWAM parts.

(3) The single-bead deposition experiments show that the applying of ELSMF can reduce the height as well as increase the width of single weld bead, the multi-bead overlapping and multi-layer multi-pass deposition experiments demonstrate that the external magnetic field can improve the surface quality of multi-layer parts.

(4) The conclusions of the above study reveal the mechanism ofAWAM processassisted by ELSMF, and it also can provide the reference for AWAM process assisted by magnetic field.

Declarations

Conflict of Interest

The authors declare that they have no conflict of interest.

Acknowledgments

This work was supported by the National Natural Science Foundation of China (Grant no. 51705287, 51775308, 51975270). The authors would like to thank Rui Wang and Feixiang Mei for their experimental contributions.

References

[1] Ding D H, Pan Z X, Cuiuri D, et al. Wire-feed additive manufacturing of metal components: technologies, developments and future interests[J]. The International Journal of Advanced Manufacturing Technology, 2015, 81(1-4): 465-481.

[2] Panda B, Shankhwar K, Garg A, et al. Evaluation of genetic programming-based models for simulating bead dimensions in wire and arc additive manufacturing[J]. Journal of Intelligent Manufacturing, 2019, 30(2): 809-820.

[3] Fu Y H, Wang G L, Zhang H O, et al. Optimization of surface appearance for wire and arc additive manufacturing of Bainite steel[J]. The International Journal of Advanced Manufacturing Technology, 2016, 91(1-4): 1-13.

[4] Xiong J, Zhang G J. Adaptive control of deposited height in GMAW-based layer additive manufacturing[J]. Journal of Materials Processing Technology, 2014, 214(4): 962-968.

[5] Li Y Z, Han Q L, Zhang G J, et al. A layers-overlapping strategy for robotic wire and arc additive manufacturing of multi-layer multi-bead components with homogeneous layers[J]. The International Journal of Advanced Manufacturing Technology, 2018, 96(9): 3331-3344.

[6] Song Y A, Park S, Choi D, et al. 3d welding and milling: part i–a direct approach for freeform fabrication of metallic prototypes[J]. International Journal of Machine Tools & Manufacture, 2005, 45(9): 1057-1062.

[7] Xie Y, Zhang H O, Zhou F. Improvement in geometrical accuracy and mechanical property for arc-based additive manufacturing using metamorphic rolling mechanism[J]. Journal of Manufacturing Science & Engineering, 2016, 138(11): 111002.

[8] Bai X W, Zhang H O, Wang G L. Electromagnetically Confined Weld-based Additive Manufacturing[J]. Procedia CIRP, 2013, 6: 516-521.

[9] Zhu S, Wang Q W, Yin F L, et al. Research on Droplet Transfer of MIG Welding with Alternating Longitudinal Magnetic Field[J]. Advanced Materials Research, 2011, 189-193:993-996.

[10] Wang L, Wu C S, Gao J Q. Suppression of humping bead in high speed GMAW with external magnetic field[J]. Science and Technology of Welding and Joining, 2016, 21(2), 131-139.

[11] Brouwer D M, Jong B R D, Boer M J D, et al. MEMS-based clamp with a passive hold function for precision position retaining of micro manipulators[J]. Journal of Micromechanics & Microengineering, 2009, 19(6):065027.

[12] Zhou X M, Tian Q H, Du Y X, et al. Study of the Influence of Longitudinal Static Magnetic Field on Surface Quality and Performances of Arc Welding Based Additive Forming Parts[J]. Journal of Mechanical Engineering, 2018, 54(2): 84-92.

[13] Chang Y L, Liu X L, Lu L, et al. Impacts of external longitudinal magnetic field on arc plasma and droplet during short-circuit GMAW[J]. International Journal of Advanced Manufacturing Technology, 2014, 70(9-12):1543-1553.

[14] Yin X Q, Gou J J, Zhang J X, et al. Numerical study of arc plasmas and weld pools for GTAW with applied axial magnetic fields[J]. Journal of Physics D Applied Physics, 2012, 45(28): 285203-285215(13).

[15] Rao Z H, Hu J, Liao S M, et al. Modeling of the transport phenomena in GMAW using argon–helium mixtures. Part I–The arc[J]. International Journal of Heat and Mass Transfer, 2010, 53(25-26): 5707-5721.

[16] Charitopoulos V M, Dua V. A unified framework for model-based multi-objective linear process and energy optimisation under uncertainty[J]. Applied Energy, 2017, 186(pt.3): 539-548.

[17] Xu G, Hu J, Tsai H L. Three-dimensional modeling of arc plasma and metal transfer in gas metal arc welding[J]. International Journal of Heat and Mass Transfer, 2009, 52(7-8): 1709-1724.

[18] Bai X W, Zhang H O, Zhou X M, et al. Electromagneto-fluid Coupling Simulation of Arc Rapid Prototyping Process with External High-frequency Magnetic Field[J]. Journal of Mechanical Engineering, 2016, 52(04): 60-66.

[19] Zhou X M, Zhang H O, Wang G L, et al. Three-dimensional numerical simulation of arc and metal transport in arc welding based additive manufacturing[J]. international journal of heat & mass transfer, 2016, 103(dec.): 521-537.

[20] Zhou X M, Zhang H O, Wang G L, et al. Simulation of the influences of surface topography of deposited layer on arc shape and state in arc based additive forming[J]. Acta Physica Sinica, 2016, 65(3)038103.

[21] Xiong J, Zhang G J, Gao, H M, et al. Modeling of bead section profile and overlapping beads with experimental validation for robotic GMAW-based rapid manufacturing[J]. Robotics & Computer Integrated Manufacturing, 2013, 29(2): 417-423.

[22] Zhou X M, Tian Q H, Du Y X, et al. Simulation of Heat and Mass Transfer in Arc Welding based Additive Forming Process with External Transverse Magnetic Field[J]. Journal of Mechanical Engineering, 2018, 54(12): 193-206.

[23] Wang Q W, Zhu S, Yin F L, et al. Numerical Simulation of MIG Welding Arc with Longitudinal Magnetic Field[J]. Materials science forum, 2012, 704-705(PT.1): p.668-673.

Figures

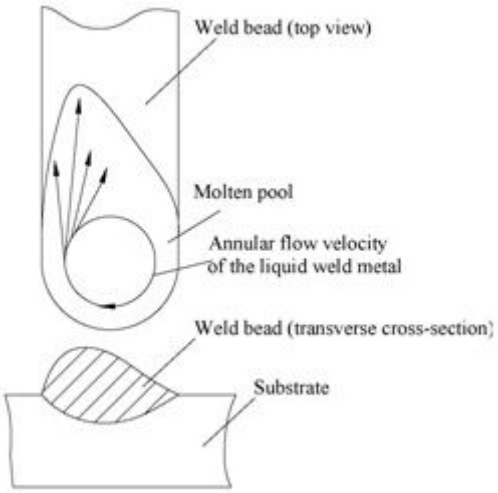

Figure 1

Schematic representation of molten pool(top view) and weld bead(transverse cross-section) in arc welding bead deposition assisted by the longitudinal static magnetic field

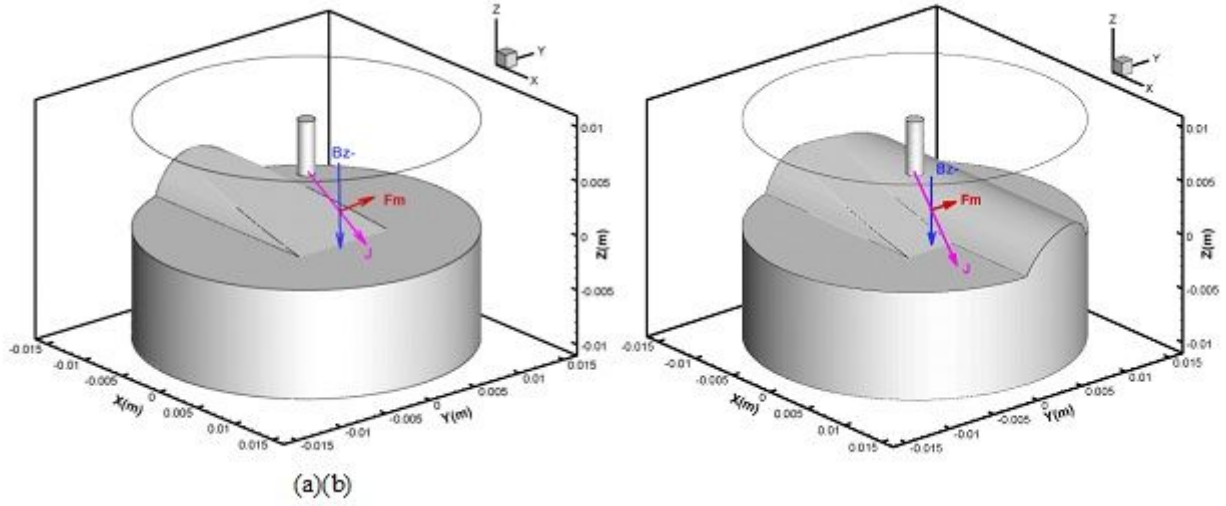

Figure 2

The diagrammatic sketch of arc models in the presence of ELSMF: (a) single-bead deposition; (b) overlapping deposition

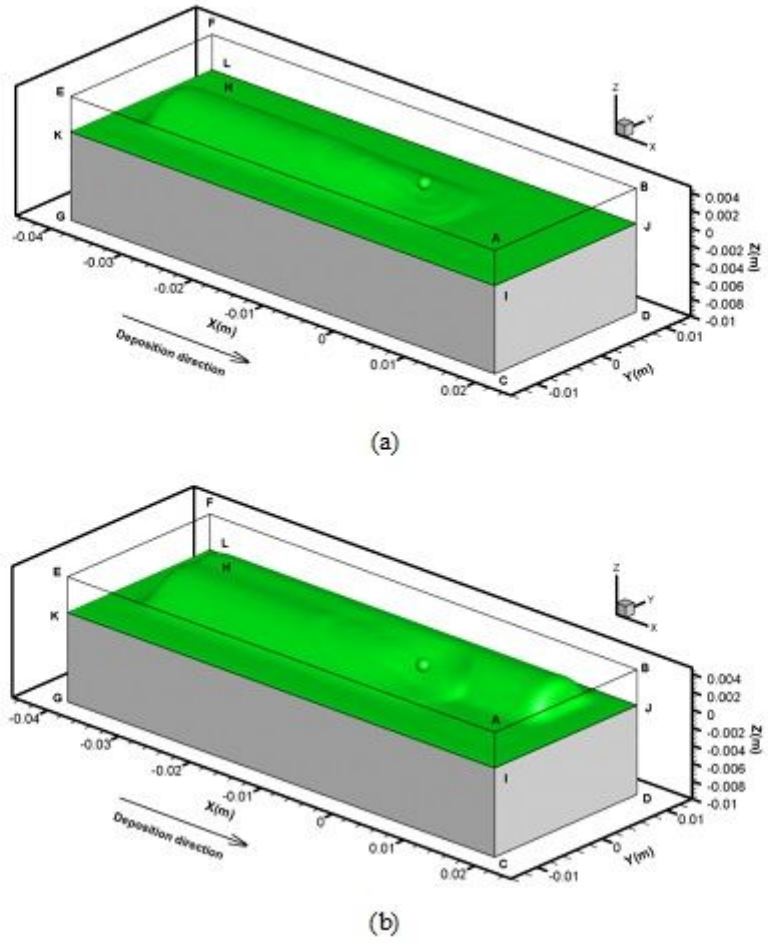

Figure 3

The schematic representation of metal transport models: (a) single-bead deposition; (b) overlapping deposition

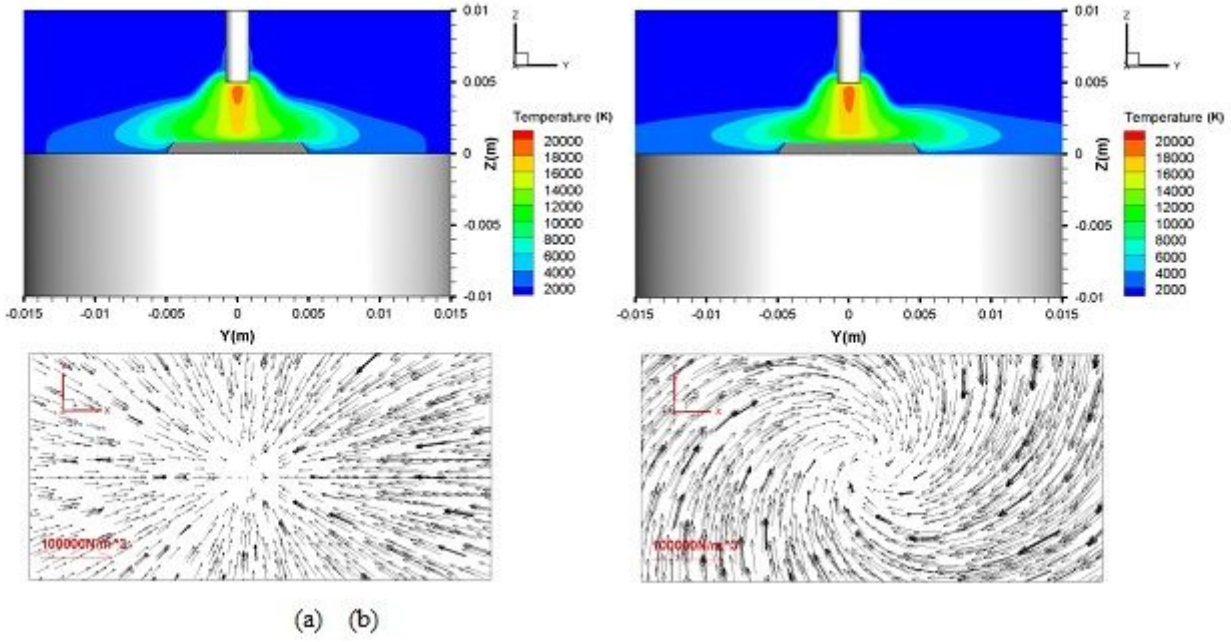

Figure 4

Simulated results of arc temperature and molten pool electromagnetic force: (a) normal single-bead deposition; (b) single-bead deposition in the presence of ELSMF.

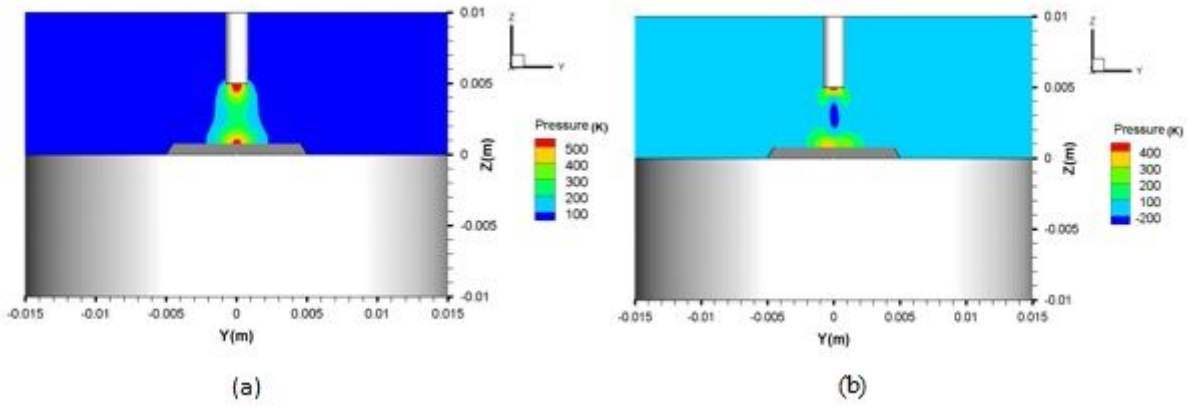

Figure 5

Simulated results of arc pressure: (a) normal single-bead deposition; (b) single-bead deposition in the presence of ELSMF.

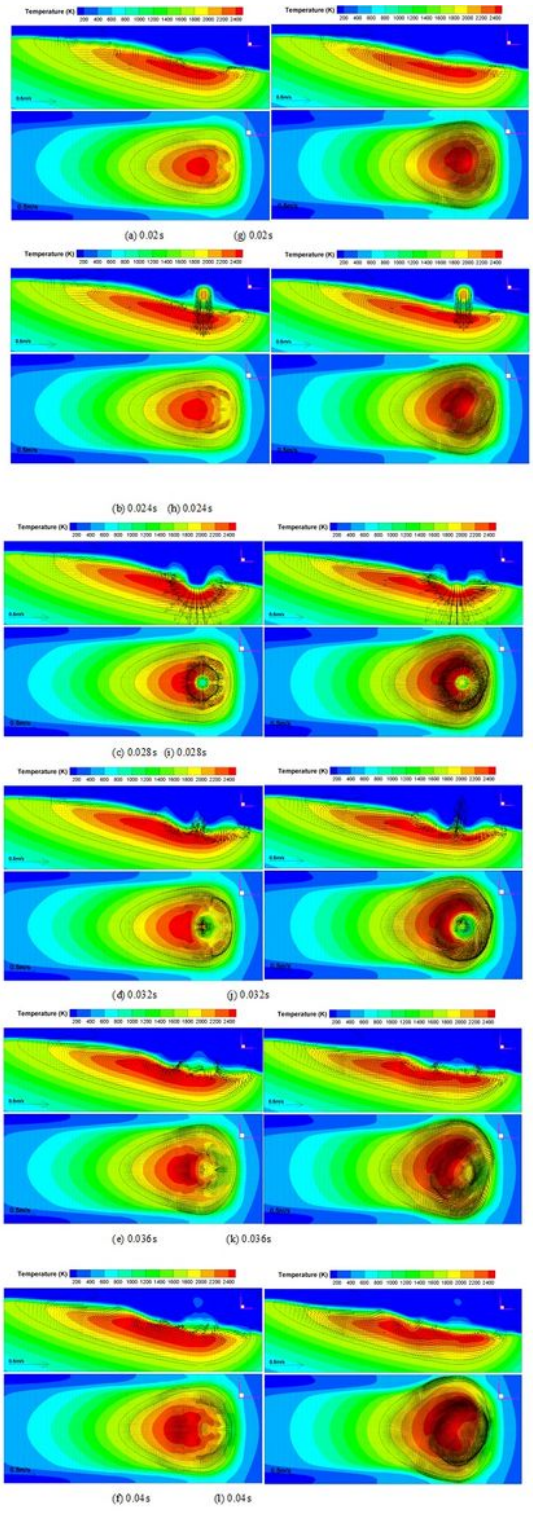

Figure 6

The temperature and velocity vector distribution: (a~f) normal single-bead molten pool from 0.02s to 0.04s, and (g~l) single-bead molten pool in the presence of ELSMF from 0.02s to 0.04s

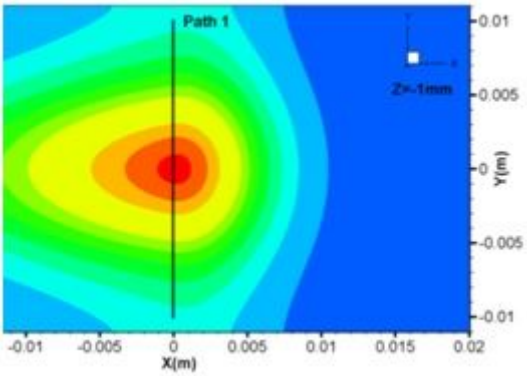

Figure 7

Schematic diagram of path 1 on Z=-1mm plane.

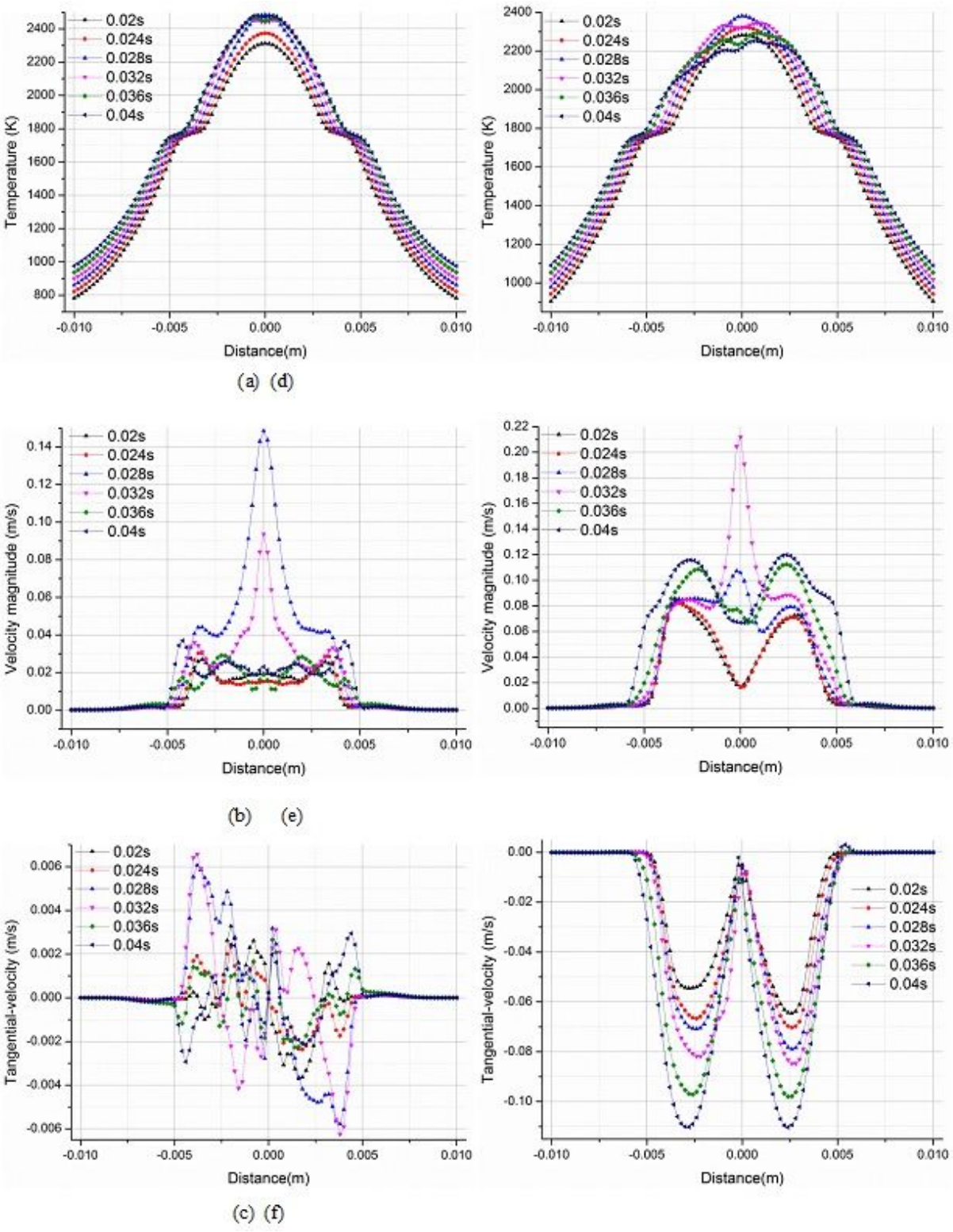

Figure 8

Distributions of temperature and velocity on path 1 at different instants: (a~c) normal single-bead deposition results , and (d~f) the single-bead deposition results in the presence of ELSMF

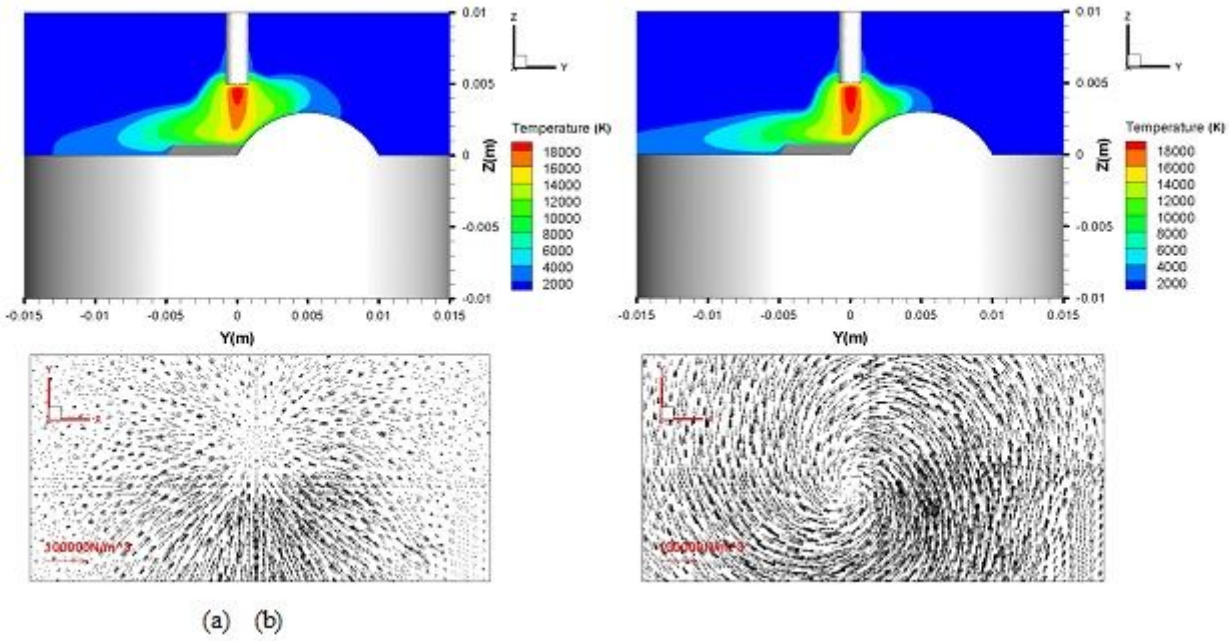

Figure 9

Simulated results of arc temperature and molten pool electromagnetic force: (a) normal overlapping deposition; (b) overlapping deposition in the presence of ELSMF.

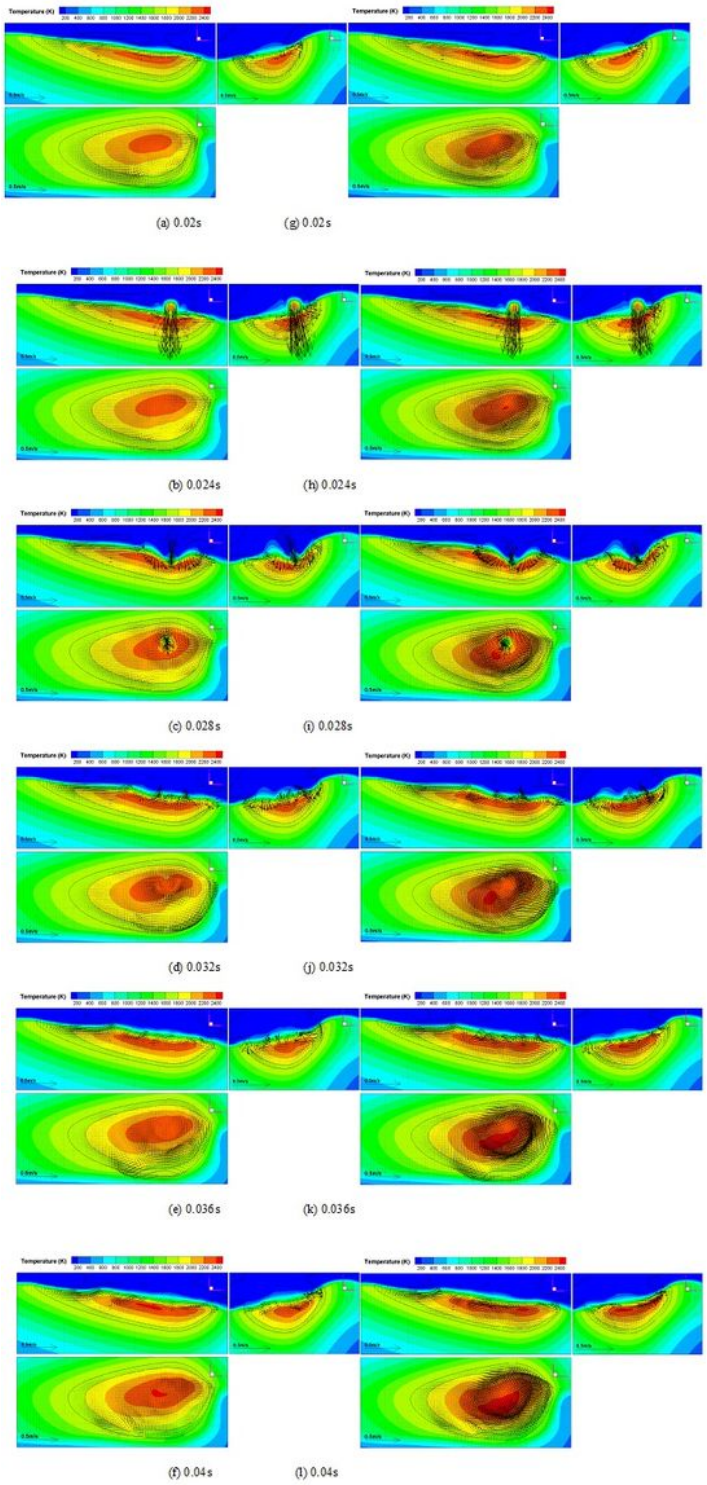

Figure 10

The temperature and velocity vector distribution: (a~f) normal overlapping molten pool from 0.02s to 0.04s, and (g~l) overlapping molten pool in the presence of ELSMF from 0.02s to 0.04s

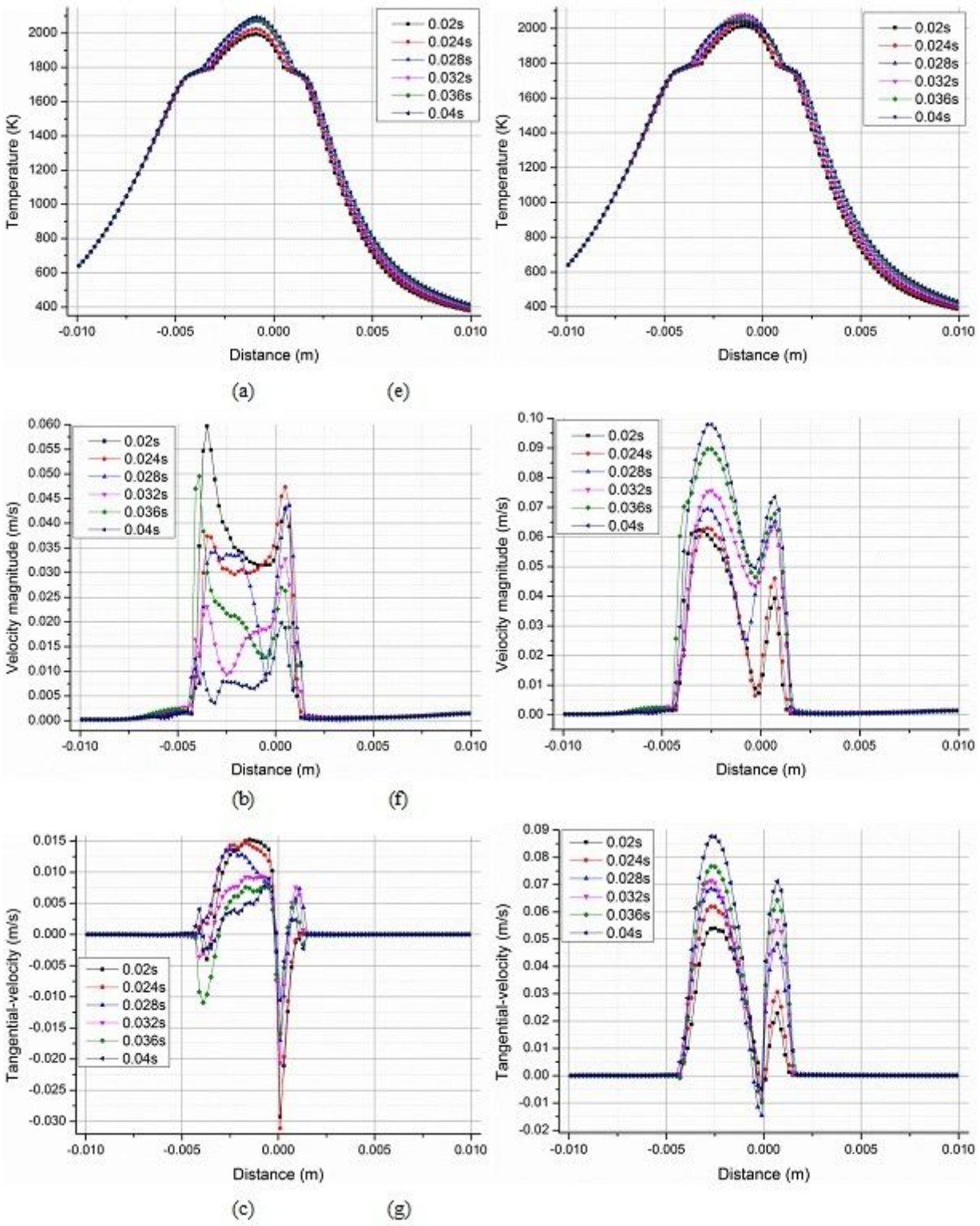

Figure 11

Distributions of temperature and velocity on path 1 at different instants: (a~d) normal overlapping deposition results , and (e~h) the overlapping deposition results in the presence of ELSMF

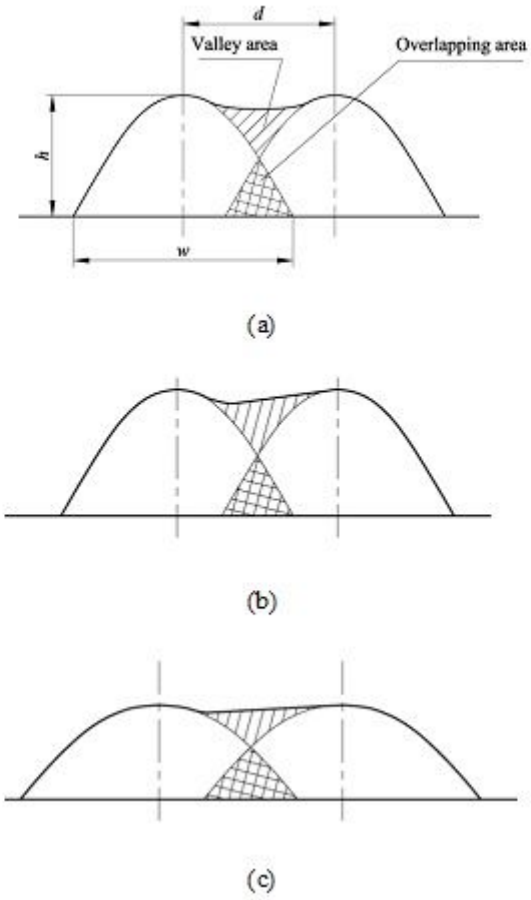

Figure 12

the schematic representation of cross-section profile of weld bead changes in overlapping deposition assisted by longitudinal magnetic field: (a) the ideal weld bead of overlapping; (b) the actual weld bead of overlapping; (c) weld bead of overlapping confined by magnetic field

Figure 13

The schematic diagram of AWAM experimental setup assisted by longitudinal magnetic field

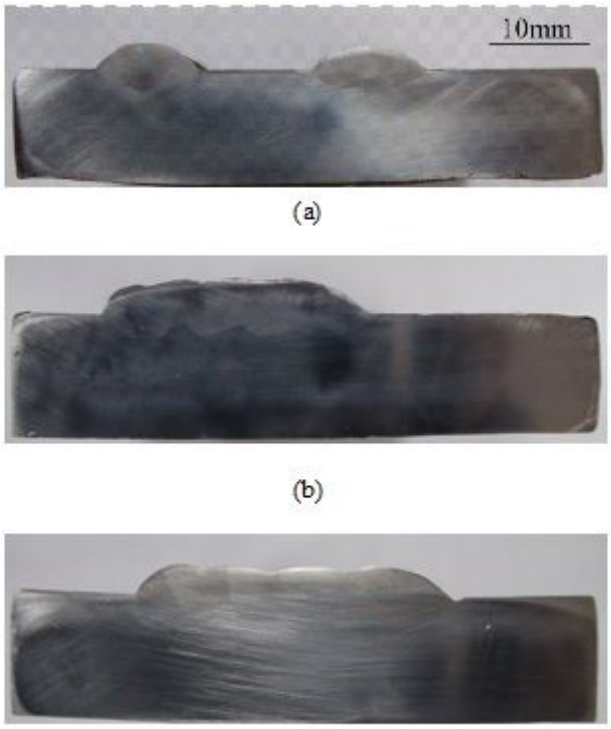

Figure 14

The cross-section of single-pass and multi-pass deposition: (a) normal single-bead deposition and single-bead deposition assisted by the longitudinal static magnetic field; (b) four pass overlapping beads of normal deposition; (c) four pass overlapping beads deposition assisted by the longitudinal static magnetic field

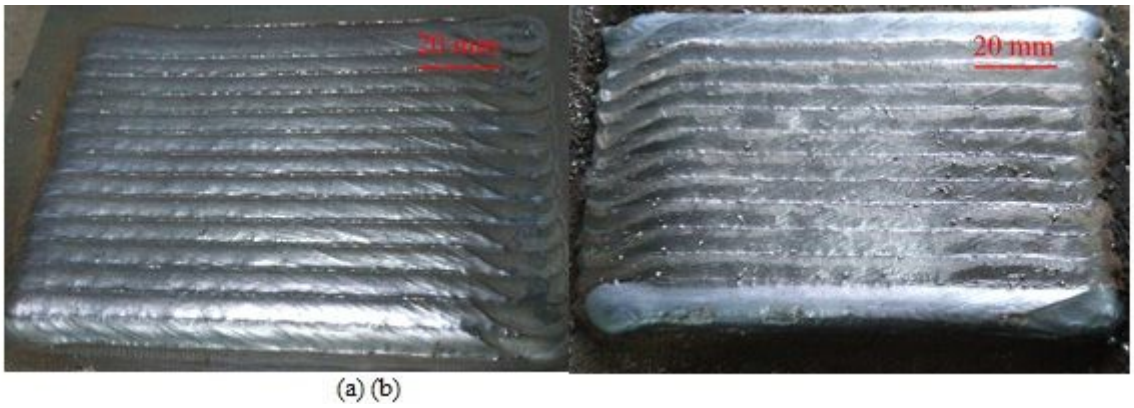

Figure 15

Comparison of surface topography of multi-layer multi-pass specimens: (a) normal deposition; (b) deposition assisted by the longitudinal static magnetic field